

Journal of Materials Chemistry A

Accepted Manuscript



This is an *Accepted Manuscript*, which has been through the Royal Society of Chemistry peer review process and has been accepted for publication.

Accepted Manuscripts are published online shortly after acceptance, before technical editing, formatting and proof reading. Using this free service, authors can make their results available to the community, in citable form, before we publish the edited article. We will replace this *Accepted Manuscript* with the edited and formatted *Advance Article* as soon as it is available.

You can find more information about *Accepted Manuscripts* in the [Information for Authors](#).

Please note that technical editing may introduce minor changes to the text and/or graphics, which may alter content. The journal's standard [Terms & Conditions](#) and the [Ethical guidelines](#) still apply. In no event shall the Royal Society of Chemistry be held responsible for any errors or omissions in this *Accepted Manuscript* or any consequences arising from the use of any information it contains.

Cite this: DOI: 10.1039/c0xx00000x

www.rsc.org/xxxxxx

Paper

Aqueous rechargeable lithium battery using $\text{NaV}_6\text{O}_{15}$ nanoflakes as a high performance anode

Dan Sun^[a], Guanhua Jin^[a], Haiyan Wang^{*[a]}, Ping Liu^[a], Yu Ren^[b], Yifan Jiang^[a], Yougen Tang^{*[a]} and Xiaobing Huang^[c]

Received (in XXX, XXX) Xth XXXXXXXXX 20XX, Accepted Xth XXXXXXXXX 20XX

DOI: 10.1039/b000000x

Poor cycling performance is still the big challenge for aqueous rechargeable lithium battery (ARLB), in which the instability of anode is considered to be the main issue. In this work, $\text{NaV}_6\text{O}_{15}$ nanoflakes were synthesized by a two-step approach and $\text{NaV}_6\text{O}_{15}/\text{LiMn}_2\text{O}_4$ ARLB system with superior cycling performance was constructed. The galvanostatic charge-discharge result demonstrates an initial discharge capacity of $110.7 \text{ mAh}\cdot\text{g}^{-1}$ (based on anode mass) at $150 \text{ mA}\cdot\text{g}^{-1}$ and the capacity retention of ca. 90% and 80% at $300 \text{ mA}\cdot\text{g}^{-1}$ after 100 and 400 cycles, respectively. Such superior cycling performance of ARLB is mainly due to the intrinsic 3-D tunneled structure of $\text{NaV}_6\text{O}_{15}$, nanoflake morphology and relatively stable electrode surface, as verified by the X-ray diffraction (XRD), electrochemical impedance spectroscopy (EIS), and scanning electron microscopy (SEM) results of the tested electrodes. Moreover, a simple single-phase reaction mechanism during the lithium ion insertion/extraction process is observed for $\text{NaV}_6\text{O}_{15}$ by XRD analysis.

1. Introduction

With the dramatically growing demand for light weight, efficient, safe and cost effective electrical energy storage systems, Li ion battery with non-aqueous electrolytes (LIBs) has been widely utilized as power sources for portable electronic devices and also attracted overwhelming attention for electric vehicles (EVs) and large-scale energy storage system^[1]. However, some drawbacks such as safety issue, low conductivity and high cost arising from the use of flammable organic electrolytes limit its further applications. It is of great importance to explore new energy storage solution to improve their safety, rate capability and reduce the cost.

In 1994, an alternative rechargeable Li ion battery with an aqueous electrolyte was first proposed by Dahn and co-workers^[2]. Compared with non-aqueous Li ion battery, the safety issue is fundamentally settled, and rigorous assembly conditions can be avoided. Furthermore, aqueous rechargeable lithium battery (ARLB) uses a weak alkaline or neutral aqueous solution as electrolyte, which is far more environmental friendly and the ionic conductivity of electrolyte is increased by several magnitudes^[3]. Hence, ARLB has attracted more and more attention in the field of electrochemical energy storage. Many commercial Li ion intercalated materials such as LiCoO_2 ^[4], LiMn_2O_4 ^[5], LiFePO_4 ^[6], $\text{LiNi}_{1/3}\text{Co}_{1/3}\text{Mn}_{1/3}\text{O}_2$ ^[7], have been well studied as cathode materials for ARLB. However, limited by the decomposition potential of water, there are relatively less suitable anode materials for ARLB^[8]. Vanadium oxides and its derivatives are considered to be ideal candidates as anode materials for ARLB due to their high capacity and suitable voltage^[9]. LiV_3O_8 is the most studied material^{[10],[9a, 9d, 11]}. However, LiV_3O_8 shows obvious capacity loss upon cycling in aqueous electrolyte. Decomposition of H_2O , material dissolution in aqueous electrolyte, and structural change of the electrode materials have been proposed as the main reasons for capacity fading^[8a, 9b, 12], in which deterioration of the crystal structure is the particular one^[9b]. Accordingly, to design a novel, high

performance anode material to further better the cycling stability of the ARLB is of great urgency.

As we know, most vanadium oxides are layered structure, and small amount of some inorganic molecules such as H_2O , CO_2 and NH_3 could integrate into the layered structure. As a result, the interlayer space expands which may lead to enhanced electrochemical properties^[13]. Moreover, because of the existing of non-covalent bonding like H-bond, the inorganic molecules can also act as a pillar to connect the neighboring layers, thus the crystal structure of materials is stabilized and cycling stability is enhanced. In view of this result, we consider that the crystal stability of vanadium oxides can be further improved if the two-dimensional (2-D) layered structure could be converted into a 3-D tunneled structure through covalent bonding which is much stronger than H-bonding. $\text{NaV}_6\text{O}_{15}$ ($\text{Na}_{0.33}\text{V}_2\text{O}_5$) owns such a rigid 3-D tunneled structure and has attracted more and more interest recently. Liu *et al.*^[14] reported single crystalline $\text{NaV}_6\text{O}_{15}$ nanorods which showed a discharge capacity as high as $328 \text{ mAh}\cdot\text{g}^{-1}$ at $20 \text{ mA}\cdot\text{g}^{-1}$ in organic electrolyte and $300 \text{ mAh}\cdot\text{g}^{-1}$ discharge capacity remaining after 70 cycles at $50 \text{ mA}\cdot\text{g}^{-1}$. Even in aqueous electrolytes, $\text{Na}_{0.33}\text{V}_2\text{O}_5$ also has good cycling performance (capacity retention of 51.2% after 100 cycles)^[15], which is better than the most of reported LiV_3O_8 ^[9a-c, 16] and $\text{VO}_2(\text{B})$ ^[2]. Although some works have been reported, more intensive studies are still necessary to further enhance the cycling performance of $\text{NaV}_6\text{O}_{15}$ in ARLB, and the Li ion insertion/extraction mechanism of $\text{NaV}_6\text{O}_{15}$ in ARLB is urgent to be understood.

It is well known that fabrication methods and morphology affect the electrochemical properties of electrode materials significantly. 2-D nanoflakes have attracted enormous attention owing to their fascinating physical and chemical properties^[17]: short diffusion length for Li^+ and e^- , low surface area in contact with the electrolyte (decrease the irreversible surface reaction)^{24,25}. Heli *et al.*^[17a] reported that LiV_3O_8 nanosheets had a higher discharge capacity in ARLB, compared to the bulk sample. While, the fabrication and morphology studies about $\text{NaV}_6\text{O}_{15}$ in ARLB are still insufficient. In this paper, a simple two-step method

using ultrathin $(\text{NH}_4)_{0.5}\text{V}_2\text{O}_5$ nanoflakes as the self-sacrifice precursor is employed to fabricate $\text{NaV}_6\text{O}_{15}$ nanoflakes. An ARLB system consisting of LiMn_2O_4 as cathode material, $\text{NaV}_6\text{O}_{15}$ as anode material, and Li_2SO_4 solution as electrolyte is constructed. This system delivers superior cycling stability with the capacity retention of 80% over 400 cycles at $300 \text{ mA} \cdot \text{g}^{-1}$. The superior cycling stability of such ARLB is well analyzed by XRD, EIS and SEM measurements. More importantly, Li ion insertion/extraction mechanism of $\text{NaV}_6\text{O}_{15}$ in aqueous electrolyte is proposed and verified in this work.

2. Experimental

2.1 Synthesis of $\text{NaV}_6\text{O}_{15}$ nanoflake.

All the starting materials were analytically pure grade and directly used without any purification. The $\text{NaV}_6\text{O}_{15}$ nanoflake was prepared by the similar method according to our early work^[28]. Well-dispersed $(\text{NH}_4)_{0.5}\text{V}_2\text{O}_5$ nanosheet fabricated by a facile hydrothermal method was used as the self-sacrifice precursor. NH_4VO_3 (1.7547 g, 99%, Tianjin Guangfu Institute of Fine Chemicals) and oxalic acid (1.0 g, 99.5%, Sinopharm Chemical Reagent Co., Ltd.) were dissolved in distilled water under gentle temperature with vigorous stirring. The yellow-green solution was then transferred into a 100 ml Teflon lined stainless steel autoclave. The autoclave was heated at 180°C for 24 h and then cooled to room temperature naturally. The obtained precipitate was filtered and washed with distilled water several times and then dried at 80°C overnight. 0.2 g of PEG-4000 was well dispersed in distilled water, then a proper amount of $(\text{NH}_4)_{0.5}\text{V}_2\text{O}_5$ and sodium hydroxide (the molar ratio of Na: V in theory is 0.5: 3) were added into the solution. The mixed solution was heated at 95°C in a hotplate with stirring to produce the dry precursor. Then the collected solid was ground by agate mortar and then further sintered at 450°C for 8 h in air to obtain $\text{NaV}_6\text{O}_{15}$.

2.2 Characterizations

All X-ray diffraction (XRD) data were examined by the X-ray diffractometer (Dandong Haoyuan, DX-2700) utilizing a $\text{Cu-K}\alpha 1$ source with a step of 0.02° . XRD measurement of electrodes was different from the examination of $\text{NaV}_6\text{O}_{15}$ powder. The whole electrode consisting of active material, Super P carbon and polytetrafluoroethylene (PTFE), after washing with deionized water and drying for several hours, was directly used to perform the XRD test and note that no signal of stainless steel mesh was observed probably due to the thick electrode film. Note that each cell was charged to 1.2 V and kept at that voltage for 2 h before disassembling. X-ray photoelectron spectroscopy (XPS) measurement was performed on the K-Alpha1063 spectrometer. The XPS patterns were collected using $\text{Al K}\alpha$ radiation at a voltage of 12 kV and current of 6 mA. Charging effect was corrected by adjusting the binding energy of C1s peak from carbon contamination to 284.5 eV. Morphological studies were conducted using a Nova NanoSEM 230 scanning electron microscopy (SEM) and a JEOL JEM-2100F transmission electron microscopy (TEM) employing a LaB_6 filament as the electron source. The BET surface area of the samples was detected by nitrogen adsorption/desorption at -196°C using a Builder SSA-4200 apparatus. The XPS fitting was performed using XPSPEAK software, and the crystal structure of $\text{NaV}_6\text{O}_{15}$ was drawn by Diamond 3.2.

2.3 Electrochemical measurements

The used LiMn_2O_4 was provided by Hunan Reshine New Material Co., Ltd. The $\text{NaV}_6\text{O}_{15}$ and LiMn_2O_4 electrodes were

made in a similar way. Tested electrodes were obtained by pressing a mixture of the active material, Super P carbon and PTFE in a weight ratio of 80:10:10 using distilled water as solvent on a stainless steel mesh and then dried at 110°C for 8 h. Cyclic voltammetry of $\text{NaV}_6\text{O}_{15}$ and LiMn_2O_4 electrodes was performed using a three electrode system, where the tested electrode was used as working electrode, platinum sheet electrode and saturated calomel electrode (SCE, 0.242 V vs. SHE: standard hydrogen electrode) as the counter and reference electrodes, respectively. Cyclic voltammetry was investigated at room temperature using an electrochemical station (CHI660D). The CR2016 coin-type cells were constructed by using LiMn_2O_4 electrode as cathode, $\text{NaV}_6\text{O}_{15}$ electrode as anode, Li_2SO_4 (2 mol L^{-1}) as electrolyte. Excessive LiMn_2O_4 , with cathode/anode mass ratio of (1.6~2)/1 is designed for exactly evaluating the electrochemical properties of $\text{NaV}_6\text{O}_{15}$. The Li_2SO_4 electrolyte is pre-treated by the flowing argon injection into the solution to eliminate the soluble oxygen. Charge and discharge tests were conducted under a desired current density by a Newware battery testing system (CT-3008W) at room temperature. Electrochemical impedance spectroscopy (EIS) was recorded by a Princeton workstation (PARSTAT2273, EG&G, US) over the frequency range from 500 kHz to 10 mHz with an amplitude of 5 mV. Before testing, the measured cell is charged to 1.2 V at $300 \text{ mA} \cdot \text{g}^{-1}$, and then held for 2 h to reach a stable state.

3. Results and discussion

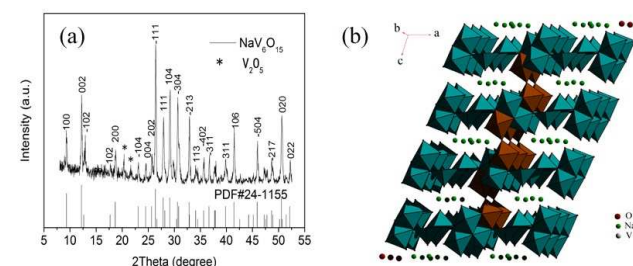


Fig. 1 (a) XRD pattern of as-prepared $\text{NaV}_6\text{O}_{15}$ and (b) crystal structure of $\text{NaV}_6\text{O}_{15}$.

The XRD pattern of $(\text{NH}_4)_{0.5}\text{V}_2\text{O}_5$ precursor obtained by one-step hydrothermal approach is shown in Fig. S1a. As seen, the main diffraction lines are consistent with standard $(\text{NH}_4)_{0.5}\text{V}_2\text{O}_5$ (JCPDS No. 18-0136) except for several tiny unknown peaks. Fig. S2 presents the SEM image of as-prepared $(\text{NH}_4)_{0.5}\text{V}_2\text{O}_5$ precursor. It shows that the precursor is composed of ultrathin nanoflakes with different sizes. The width of large nanoflakes can reach $\sim 1.5 \mu\text{m}$, and the small ones can be just $\sim 0.2 \mu\text{m}$. The length of the large one is up to several micrometers. The XRD pattern of the final product $\text{NaV}_6\text{O}_{15}$ is shown in Fig. 1a. As displayed, the main peaks could be well indexed into the monoclinic layered $\text{NaV}_6\text{O}_{15}$ phase (JCPDS No. 24-1155) with lattice parameters $a = 1.0065 \text{ nm}$, $b = 0.3597 \text{ nm}$, $c = 1.5377 \text{ nm}$, and $\beta = 109.59^\circ$ (space group: A2/m (12)), in good agreement with the reference value^{[14] [18]}. Several impurity peaks from V_2O_5 are found. Note that the impurity peaks are very weak, indicating the low content of V_2O_5 . It is known that V_2O_5 owns excellent electrochemical properties^[19], thus a slight amount of V_2O_5 impurity could be accepted. The crystal structure of $\text{NaV}_6\text{O}_{15}$ is given in Fig. 1b and Fig. S3. The quadruple VO_6 octahedra and VO_5 distorted trigonal bipyramids share the edges and corners to form a continuous $[\text{V}_6\text{O}_{15}]_n$ layer, and two VO_6 octahedra (marked with brown color) at different layers act as pillars to connect the layers by corner-shared oxygen, which form a rigid 3-D tunneled structure^{[20],[21]}. As observed, such special rigid 3-D

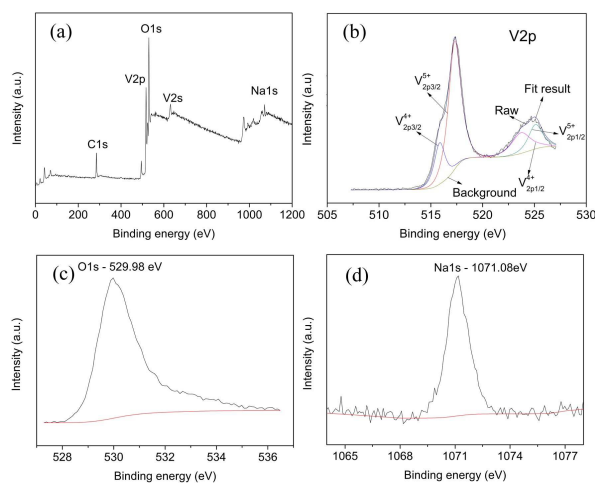


Fig. 2 XPS spectra of as-prepared $\text{NaV}_6\text{O}_{15}$.

tunneled structure is different from other 2-D layer vanadium oxides like LiV_3O_8 ^[22] and NaV_3O_8 ^[23]. This optimized structure should be comparatively rigid to avoid the loss of their long-range and partial amorphism during lithium insertion and extraction, which was described as the “pillar effect”^[15]. In fact, $\text{NaV}_6\text{O}_{15}$ with good electrochemical properties has been reported as cathode materials for Li ion battery^[14, 18b, 24].

The chemical composition and valence state of as-prepared product were further investigated by XPS. Fig. 2a is the XPS survey spectrum of $\text{NaV}_6\text{O}_{15}$. The peaks of V2p, Na1s, and O1s can be clearly seen^[25]. The high resolution XPS of V2p is displayed in Fig. 2b. As seen, it could be fitted into two pairs of peaks at 517.38 eV and 525.18 eV, corresponding to the contribution from $\text{V}^{5+}2p_{3/2}$ and $\text{V}^{5+}2p_{1/2}$, respectively^[26], while peaks located at 515.88 eV and 523.78 eV with less intensity indicate the existence of certain amount of V^{4+} . The calculated molar ratio of V^{4+} to V^{5+} is 1:5, which agrees well with the valence of V in $\text{NaV}_6\text{O}_{15}$. Peaks at 1071.0 eV (Fig. 2c) and 530.0 eV (Fig. 2d) correspond to Na1s and O1s electrons, respectively. The results from XPS analysis further confirm the formation of $\text{NaV}_6\text{O}_{15}$.

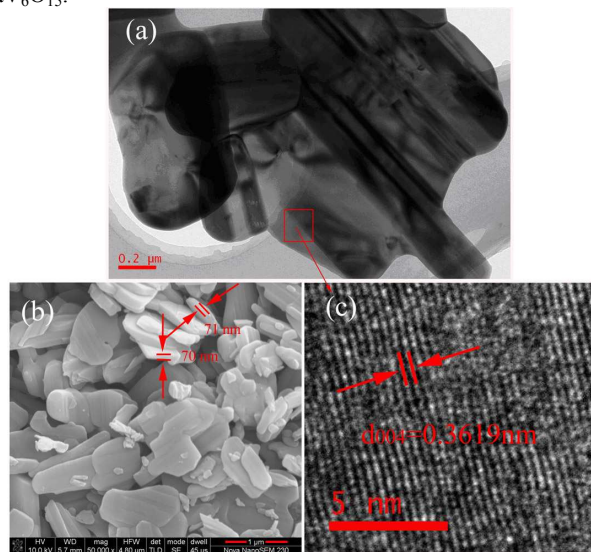


Fig. 3 TEM (a), SEM (b), and HRTEM images (c) of as-prepared $\text{NaV}_6\text{O}_{15}$.

The morphology of as-prepared $\text{NaV}_6\text{O}_{15}$ was studied by TEM and SEM (Fig. 3). The nanoflake morphology is well maintained

after the calcination of $(\text{NH}_4)_{0.5}\text{V}_2\text{O}_5$ with NaOH although certain agglomeration happens. Although the thickness of the flakes is increased, it is still less than 100 nm, as marked in Fig. 3b. The size of nanoflakes is decreased to ~ 400 nm in width, ~ 800 nm in length. The precursor shows an important impact on the morphology, structure and electrochemical properties of resultant product. The concept of a topotactic intercalation mechanism from layered structured $\text{H}_2\text{V}_3\text{O}_8$ nanowires to LiV_3O_8 nanowires has been proposed by Xu and co-workers^[27]. Here, both $(\text{NH}_4)_{0.5}\text{V}_2\text{O}_5$ precursor and $\text{NaV}_6\text{O}_{15}$ are monoclinic structure. The similar layered structures would promise the successful intercalation of Na ions without the flake-morphology destroying. The HRTEM image (Fig. 3c) of the individual nanoflakes displays clear lattice fringes with a spacing of 0.3619 nm, which corresponds to the (004) lattice plane of monoclinic $\text{NaV}_6\text{O}_{15}$ structure in Fig. 1a. The dissolution of electrode is an important reason for capacity loss of anode materials^[8a, 11]. Minimizing the surface area is an effective way to suppress the dissolution of metal ions in electrode materials. In this work, the Brunauer-Emmett-Teller (BET) surface area of as-prepared $\text{NaV}_6\text{O}_{15}$ nanoflake (Fig. S4) is $10.2 \text{ m}^2 \cdot \text{g}^{-1}$, which is a reasonable value for flake-like materials^[28].

Li ion intercalation/deintercalation behavior of $\text{NaV}_6\text{O}_{15}$ and LiMn_2O_4 electrodes in aqueous electrolyte was investigated by CV measurement (Fig. 4a), respectively. $\text{NaV}_6\text{O}_{15}$ demonstrates three reduction peaks (~ -1.0 V, -0.3 V and 0.1 V) between 0.4 and -1.0 V. The corresponding oxidation peaks are located at ~ -0.3 V, 0 V, and 0.2 V. Such a multi-step Li-ion insertion and extraction process in aqueous solution is similar to that in organic electrolyte, and it may be due to the different occupation sites of the Li ions in the host^[29]. Results above imply that $\text{NaV}_6\text{O}_{15}$ could be used as a promising intercalation anode for ARLB. Not all cathode materials showed the best stability in neutral electrolyte, for example, $\text{LiNi}_{1/3}\text{Co}_{1/3}\text{Mn}_{1/3}\text{O}_2$ were more stable in Li_2SO_4 solution with $\text{pH}=11$ because of less H^+ intercalation^[7]. Our previous work suggested that sodium vanadate as anode possesses the best cycling stability in neutral electrolyte^[8b]. And LiFePO_4 and LiMn_2O_4 could also keep stable when cycling in neutral solution^[30]. Accordingly, commercial LiMn_2O_4 was directly used as the cathode considering its relatively high intercalated potential and low cost. As seen from Fig. 4a, two pairs of redox peaks are located at ~ 0.8 V and ~ 0.92 V for LiMn_2O_4 , which agree well with the two steps of Li ion deintercalation/intercalation process in organic electrolyte. $\text{NaV}_6\text{O}_{15}/\text{LiMn}_2\text{O}_4$ ARLB (Fig. 4b) shows reversible but complicated lithium insertion /extraction behavior. There are two main oxidation peaks at *ca.* 0.75 and 1.20 V, while the corresponding reduction peaks are at *ca.* 0.58 and 1.02 V. No obvious peaks corresponding to the evolution of hydrogen and oxygen are observed, consistent with the high Coulombic efficiency in Fig. 4c. The rate performance of ARLB is investigated (Fig. 4e). A discharge capacity of $110 \text{ mAh} \cdot \text{g}^{-1}$ (based on anode mass) at $150 \text{ mA} \cdot \text{g}^{-1}$ is obtained, however, discharge capacity is decreased to $49 \text{ mAh} \cdot \text{g}^{-1}$ at $1200 \text{ mA} \cdot \text{g}^{-1}$, indicating the ordinary rate performance, which should be mainly limited by $\text{NaV}_6\text{O}_{15}$ anode. Although the rate capability is better than those of LiV_3O_8 ^[11], $\text{Li}_{1.2}\text{V}_3\text{O}_8$ ^[31] and $\text{Na}_2\text{V}_6\text{O}_{16} \cdot x\text{H}_2\text{O}$ ^[8b], it is still not a satisfactory result for application. Decreasing the thickness of flakes is considered as an effective approach for further improvement of rate performance. Note that the reversible capacity of $\text{NaV}_6\text{O}_{15}$ in ARLB is far less than that in LIBs. A similar phenomenon is also reported for LiV_3O_8 ^[9a, 9d, 10-11]. The long cycling performance of $\text{NaV}_6\text{O}_{15}/\text{LiMn}_2\text{O}_4$ at 1C is shown

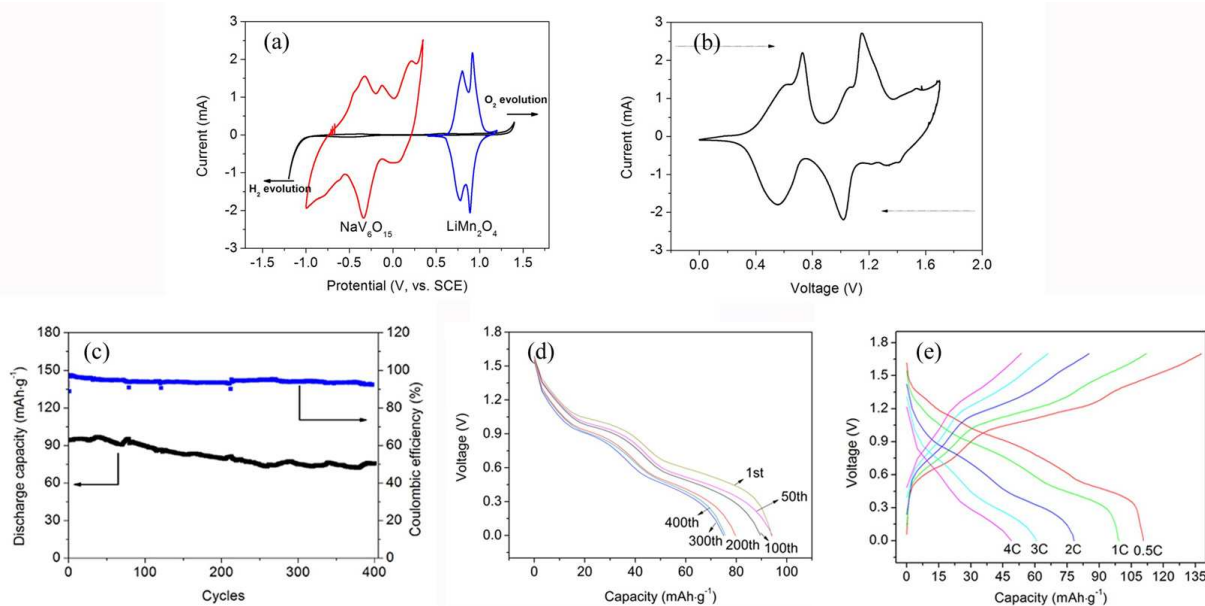


Fig. 4 (a) Cyclic voltammetry (CV) curves of $\text{NaV}_6\text{O}_{15}$ and LiMn_2O_4 electrode in Li_2SO_4 solution at a scan rate of $0.2 \text{ mV}\cdot\text{s}^{-1}$, respectively, measured by a three-electrodes system using platinum sheet as counter electrode and saturated calomel as reference electrode, (b) CV curve of $\text{NaV}_6\text{O}_{15}/\text{LiMn}_2\text{O}_4$ ARLB at a scan rate of $0.2 \text{ mV}\cdot\text{s}^{-1}$, (c) cycling performance and Coulombic efficiency of $\text{NaV}_6\text{O}_{15}/\text{LiMn}_2\text{O}_4$ at $300 \text{ mA}\cdot\text{g}^{-1}$, (d) the corresponding discharge curves of $\text{NaV}_6\text{O}_{15}/\text{LiMn}_2\text{O}_4$ at different cycles, and (e) charge-discharge curves of $\text{NaV}_6\text{O}_{15}/\text{LiMn}_2\text{O}_4$ cycled at various rates from 150 to $1200 \text{ mA}\cdot\text{g}^{-1}$.

in Fig. 4c. As seen, it shows an initial discharge capacity of $96 \text{ mAh}\cdot\text{g}^{-1}$, and in the first 100 and 200 cycles, the capacity retention is *ca.* 90% and 80%, respectively. It is worth pointing out that almost no capacity fading is observed in the later 200 cycles. The cycling stability here is superior to all reported vanadium oxides or vanadates as anode materials so far, such as $\text{Na}_{0.33}\text{V}_2\text{O}_5$ ^[15], $\text{Na}_2\text{V}_6\text{O}_{16}\cdot x\text{H}_2\text{O}$ ^[8b], $\text{VO}_2(\text{B})$ ^[2], LiV_3O_8 ^[11,13]. $\text{VO}_2(\text{B})/\text{LiMn}_2\text{O}_4$ reported by Dahn and co-workers^[2] can only be cycled for 25 cycles. When LiV_3O_8 was used as anode, the cycling stability was improved, but still far insufficient for practical application. $\text{LiV}_3\text{O}_8/\text{LiMn}_2\text{O}_4$ showed 53.5% of the initial capacity after 100 cycles and 36.7% after 220 cycles^[9d]. $\text{Na}_2\text{V}_6\text{O}_{16}\cdot 0.14\text{H}_2\text{O}/\text{LiMn}_2\text{O}_4$ with capacity retention of 77% after 200 cycles was demonstrated in our group^[8b]. The cycling performance of $\text{NaV}_6\text{O}_{15}/\text{LiMn}_2\text{O}_4$ is also better than those using coated anodes, *e.g.* polyaniline modified $\text{Li}_x\text{V}_2\text{O}_5/\text{LiMn}_2\text{O}_4$ (80% after 40 cycles at 0.2 C)^[32], polypyrrole modified $\text{Li}_x\text{V}_2\text{O}_5/\text{LiMn}_2\text{O}_4$ (82% after 60 cycles at 0.2 C)^[33], NiO modified $\text{LiV}_3\text{O}_8/\text{LiMn}_2\text{O}_4$ (81.6% after 100 cycles at $300 \text{ mA}\cdot\text{g}^{-1}$)^[34]. Noted that $\text{LiTi}_2(\text{PO}_4)_3/\text{LiMn}_2\text{O}_4$ reported by Xia *et al.* exhibited 82% of capacity retention after 200 cycles at a current rate of $10 \text{ mA}\cdot\text{cm}^{-2}$ ^[8c].

Decomposition of water in aqueous electrolyte^[8a] and the interaction between the aqueous electrolyte and electrode surface^[10] often result in relatively low Coulombic efficiency^[8d], which are regarded as an important origin of capacity fading for ARLB. In this work, as shown in Fig. 4c, the overall average Coulombic efficiency of $\text{NaV}_6\text{O}_{15}/\text{LiMn}_2\text{O}_4$ is exceeding 92%, which is much higher than that (75%) in ref.^[2] and 86% in ref.^[10]. Fig. 4d presents the corresponding discharge curves after different cycles. The discharge plateaus around 0.98 V and 0.55

V agree well with CV result. Apart from the discharge platform shrinkage in the first 200 cycles, no obvious change is observed in the later 200 cycles. Clearly, $\text{NaV}_6\text{O}_{15}/\text{Li}_2\text{SO}_4/\text{LiMn}_2\text{O}_4$ ARLB owns superior cycling stability.

XRD, EIS and SEM measurements were employed to research the origins of the superior cycling stability of $\text{NaV}_6\text{O}_{15}/\text{LiMn}_2\text{O}_4$. Fig. 5a shows Nyquist plots of the full cell after different cycles. As displayed, the plots consist of a depressed semicircle in the high frequency regions and a straight line in the low frequency region. The semicircle at high frequency can be assigned to the charge-transfer impedance (R_{ct}) on electrode-electrolyte interface, while the line region corresponds to the Warburg impedance, which reflects Li ion diffusion in the solid state electrodes^[35]. With the cycle increasing, the R_{ct} impedance increases slowly (See Table S1), probably related to the 20% capacity fading in the first 200 cycles. Increase of R_{ct} was considered as the important factor for the capacity fading of cathode materials^[36]. Liu *et al.*^[35a] considered that the improved electrochemical performance of polypyrrole-coated LiV_3O_8 could be resulted from the lower R_{ct} . Although the R_{ct} in this work involves the contributions both from cathode and anode and we still have no direct evidence to show which part is more important, one conclusion could be made that the contribution from $\text{NaV}_6\text{O}_{15}$ anode is small since the total resistance change is not obvious. It's well known that charge transfer resistance involves many factors such as electronic conductivity, crystal structure, the inter-particle contacts and electrode surface condition^[37]. Therefore, in this work, the structure and surface morphology change of electrode after different cycles are investigated in details as well.

Cite this: DOI: 10.1039/c0xx00000x

www.rsc.org/xxxxxx

Paper

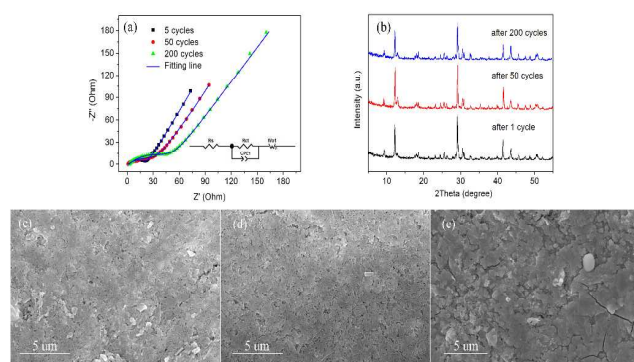


Fig. 5 (a) Electrochemical impedance spectroscopy of $\text{NaV}_6\text{O}_{15}/\text{Li}_2\text{SO}_4/\text{LiMn}_2\text{O}_4$ ARLB after different cycles at $300 \text{ mA}\cdot\text{g}^{-1}$. (b) XRD patterns of $\text{NaV}_6\text{O}_{15}$ electrodes after different cycles at $300 \text{ mA}\cdot\text{g}^{-1}$. Before disassembling, each cell was charged to 1.2 V and then kept at that voltage for 2 h. SEM images of $\text{NaV}_6\text{O}_{15}$ electrode after 3 cycles (c), 50 cycles (d), and 400 cycles (e) at $300 \text{ mA}\cdot\text{g}^{-1}$.

Fig. 5b shows the XRD patterns of $\text{NaV}_6\text{O}_{15}$ electrodes after different cycles (1, 50, 200). Apart from intensity change in some diffraction peaks, which is probably due to the smooth surface of the electrode film^[38], the XRD patterns of electrodes are similar to $\text{NaV}_6\text{O}_{15}$ powder in Fig. 1a. The XRD patterns of $\text{NaV}_6\text{O}_{15}$ electrodes after 200 cycles show no visible structure change, degradation or new impurity peaks, compared with the one after 1 cycle. As we know, the structure transformation of vanadates is a main cause for capacity fading. Köhler *et al.*^[9b] found that XRD pattern of LiV_3O_8 after 100 cycles appeared additional peaks compared with that without cycling. Wang *et al.*^[32] reported that crystalline structure of $\text{Li}_x\text{V}_2\text{O}_5$ changed and became nearly amorphous after 40 cycles. Here, the stable cycling behavior of $\text{NaV}_6\text{O}_{15}$ electrode during the cycling should be related to its 3-D tunneled structure as mentioned above in Fig. 1a. There are VO_6 octahedra act as the “pillar” to connect the $[\text{V}_6\text{O}_{15}]_n$ layers by corner-shared oxygen atoms and change the 2D layered structure into a 3D tunneled structure. As a result, structure collapse and crystallinity loss are effectively alleviated during repetitive electrochemical lithiation. Xie *et al.*^[15] indicated that the capacity retention of 3-D tunneled $\text{Ag}_{0.33}\text{V}_2\text{O}_5$ after 50 cycles was 71.4%, while that of 2-D layered $\text{Ag}_2\text{V}_4\text{O}_{11}$ was only 27.5%. The

corresponding XRD patterns (Fig. S5) of LiMn_2O_4 after different cycles also indicate no observable structure degradation. As reported by Wu *et al.*^[39], LiMn_2O_4 in aqueous electrolyte using activated carbon as counter electrode could be well cycled even up to 10000 cycles. In addition, nanoflake morphology of $\text{NaV}_6\text{O}_{15}$ could be regarded as another important factor. It is well known that morphologies of active materials also affect the cycling stability significantly. During the Li ions insertion/extraction, crystal volume would expand and then contract to some extent, probably resulting in broken particles. There is no doubt that 2-D morphology (nanoflake or nanosheet) could tolerate more serious structural variations during Li ion insertion/extraction process, leading to a better cycling stability^[17b, 40]. Meanwhile, the surface area ($10.2 \text{ m}^2\cdot\text{g}^{-1}$) of nanoflakes would decrease the irreversible surface reaction, which is beneficial to the cycling performance. Fig. 5(c, d, e) presents the surface morphology of $\text{NaV}_6\text{O}_{15}$ electrode after 1, 50, and 400 cycles at 1C rate. As displayed, the surface of $\text{NaV}_6\text{O}_{15}$ electrodes after 1 and 50 cycles is almost the same. After 400 cycles, the surface of electrode still remains well, though a tiny change. It is noted that the surface integrity of the electrode is slightly decreased and several voids are observed. Because of the attacking of H_2O ^[8c], dissolution of surface active materials, an important reason for capacity fading of ARLB, could not be ignored^[11]. Based on the XRD, EIS and SEM results, it could be deduced that the increase of R_{ct} is mainly originated from the tiny change in electrode surface, not the crystal structure. In this work, a relatively stable electrode surface of $\text{NaV}_6\text{O}_{15}$ electrode implies that the dissolution of active material could be effectively suppressed, thus leading to excellent cycling performance. Similar results have been reported in ref. ^[41]

As a novel anode for ARLB, it is of importance to study the Li-ion insertion/extraction mechanism of $\text{NaV}_6\text{O}_{15}$ electrode. XRD patterns of $\text{NaV}_6\text{O}_{15}$ electrodes at different states in the first two cycles (marked in Fig. 6A) are investigated and displayed in Fig. 6B. All the electrodes still exhibit monoclinic structure, similar to as-prepared $\text{NaV}_6\text{O}_{15}$ powder in Fig. 1a. Upon closer observation, we find that during the charge process (a - c), the diffraction peak (104) shifts toward the low angle direction

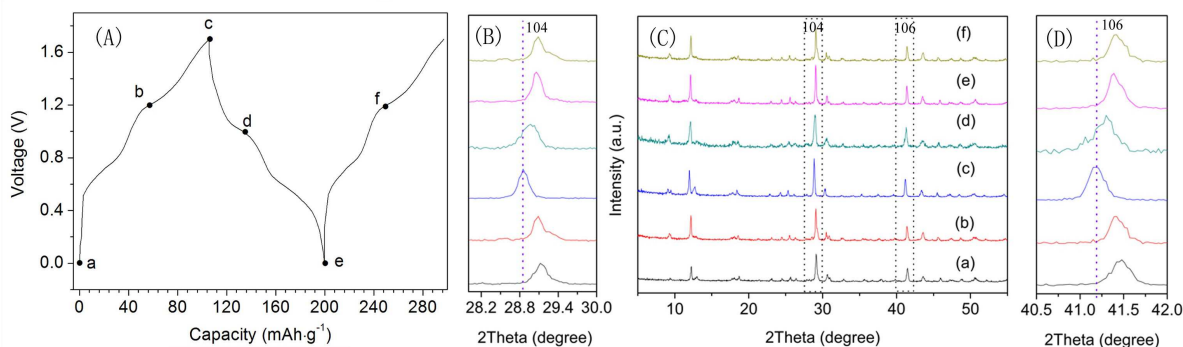


Fig. 6 (A) The charge-discharge curves of $\text{NaV}_6\text{O}_{15}/\text{Li}_2\text{SO}_4/\text{LiMn}_2\text{O}_4$ ARLB at 1C. (B) XRD patterns of $\text{NaV}_6\text{O}_{15}$ at different voltages: a - 0 V, b - 1.2 V, c - 1.7 V, d - 1.0 V, e - 0 V, f - 1.2 V at 1C. Patterns in (B) and (D) are the partially enlarged portions of the highlighted parts in (C).

Cite this: DOI: 10.1039/c0xx00000x

www.rsc.org/xxxxxx

Paper

slightly, while diffraction peak (106) shifts toward the high angle direction gradually. This phenomenon is related to the change of lattice parameters, as presented in Table S2. During the charge process, *a* axis in unit crystal increases gradually, resulting in the expansion of crystal volume. While during the discharging process (c - e), the diffraction peaks (104) and (106) shift back finally, *a* axis contracts and crystal volume decreases (Fig. 8C). A similar charge and discharge process is also found in LiMn₂O₄ (Fig. S6). Because of the intrinsic crystal structure, the volume of NaV₆O₁₅ inserted with Li ions (a, 0.5265 nm³) expands slightly (~ 2%) compared with that of NaV₆O₁₅ nanoflakes (c, 0.5379 nm³). The small structural variation further supports the stability of as-prepared NaV₆O₁₅ nanoflakes. More importantly, only one phase is observed along the lithium insertion/extraction process, which is in accord with that of β-Na_{0.33}V₂O₅ in nonaqueous electrolyte^[18b], so the reaction equation in the anode can be expressed as follow:



Such a simple single-phase mechanism is different from LiV₃O₈, for which irreversible phase transforming between LiV₃O₈ and Li₄V₃O₈ is considered as a capacity fading reason^{[42],[43]}.

Conclusions

In summary, NaV₆O₁₅ nanoflakes have been synthesized using (NH₄)_{0.5}V₂O₅ as self-sacrifice precursor. ARLB of NaV₆O₁₅/LiMn₂O₄ was constructed and showed the superior cycling stability. At 150 mA·g⁻¹, the ARLB exhibited an initial discharge capacity of 110.7 mAh·g⁻¹, when the current density was up to 300 mA·g⁻¹, discharge capacity of 97 mAh·g⁻¹ remained, and the capacity retention over 400 cycles was ca. 80%. Results revealed that the excellent cycling stability could be attributed to the rigid 3-D tunneled structure of NaV₆O₁₅, nanoflake morphology and relatively stable electrode surface. Moreover, a simple single-phase reaction mechanism during the Li ion insertion/extraction was first proposed for NaV₆O₁₅ in ARLB. The superior electrochemical performance of NaV₆O₁₅ nanoflake indicates its potential application in ARLB.

Acknowledgements

Financial supports from the National Nature Science Foundation of China (No.21301193 and No.51304077), China Postdoctoral Science Foundation Funded Project (No.2013M 530356), Fundamental Research Funds for the Central Universities of Central South University and Hunan Provincial Natural Science Foundation of China (No. 14JJ3022 and No.13JJ4100) are greatly appreciated.

Notes and References

^a College of Chemistry and Chemical Engineering, Central South University, Changsha, 410083, P.R. China. Tel.: +86-731-88830 886; Fax: +86-731-88879616. E-mail: wanghy419@126.com; ygtang@csu.edu.cn.

^b New Energy Center, National Institute of Clean-and-low-carbon Energy, Beijing, 102209, P.R. China

^c College of Chemistry and Chemical Engineering, Hunan University of Arts and Science, Changde 415000, P.R. China

† Electronic Supplementary Information (ESI) available: [XRD pattern and SEM image of as-prepared (NH₄)_{0.5}V₂O₅ precursor; Crystal structure along the different axis; N₂ adsorption-desorption isotherm of the NaV₆O₁₅ nanoflake; XRD patterns of LiMn₂O₄ electrodes after different cycles; XRD patterns of LiMn₂O₄ at different cell voltages; Calculated crystal parameter of NaV₆O₁₅ at different cell voltages]. See DOI: 10.1039/b000000x/

- [1] aJ. M. Tarascon, M. Armand, *Nature* 2001, 414, 359-367; bM. Armand, J. M. Tarascon, *Nature* 2008, 451, 652-657.
- [2] W. Li, J. R. Dahn, D. S. Wainwright, *Science (New York, N.Y.)* 1994, 264, 1115-1118.
- [3] G. J. Wang, Q. T. Qu, B. Wang, Y. Shi, S. Tian, Y. P. Wu, R. Holze, *J. Power Sources* 2009, 189, 503-506.
- [4] aR. Ruffo, C. Wessells, R. A. Huggins, Y. Cui, *Electrochem. Commun.* 2009, 11, 247-249; bG. J. Wang, L. C. Yang, Q. T. Qu, B. Wang, Y. P. Wu, R. Holze, *J. Solid State Electr.* 2010, 14, 865-869; cR. Ruffo, F. La Mantia, C. Wessells, R. A. Huggins, Y. Cui, *Solid State Ionics* 2011, 192, 289-292.
- [5] Y. Cui, Z. Yuan, W. Bao, Q. Zhuang, Z. Sun, *J. Appl. Electrochem.* 2012, 42, 883-891.
- [6] P. He, J. L. Liu, W. J. Cui, J. Y. Luo, Y. Y. Xia, *Electrochim. Acta* 2011, 56, 2351-2357.
- [7] Y. Wang, J. Luo, C. Wang, Y. Xia, *J. Electrochem. Soc.* 2006, 153, A1425-A1431.
- [8] aY. Wang, J. Yi, Y. Xia, *Adv. Energy Mater.* 2012, 2, 830-840; bD. Zhou, S. Liu, H. Wang, G. Yan, *J. Power Sources* 2013, 227, 111-117; cJ. Y. Luo, Y. Y. Xia, *Adv. Funct. Mater.* 2007, 17, 3877-3884; dH. Wang, K. Huang, Y. Zeng, S. Yang, L. Chen, *Electrochim. Acta* 2007, 52, 3280-3285.
- [9] aL. Liu, F. Tian, Z. Yang, X. Wang, M. Zhou, X. Wang, *J. Phys. Chem. Solids* 2011, 72, 1495-1500; bJ. Köhler, H. Makihara, H. Uegaito, H. Inoue, M. Toki, *Electrochim. Acta* 2000, 46, 59-65; cG. Wang, L. Fu, N. Zhao, L. Yang, Y. Wu, H. Wu, *Angew. Chem. Int. Ed.* 2007, 46, 295-297; dG. J. Wang, H. P. Zhang, L. J. Fu, B. Wang, Y. P. Wu, *Electrochem. Commun.* 2007, 9, 1873-1876.
- [10] M. Zhao, Q. Zheng, F. Wang, W. Dai, X. Song, *Electrochim. Acta* 2011, 56, 3781-3784.
- [11] A. Caballero, J. Morales, O. A. Vargas, *J. Power Sources* 2010, 195, 4318-4321.
- [12] Y. Wang, J. Yi, Y. Xia, *Adv. Energy Mater.* 2012, 2, 830-840.
- [13] V. Manev, A. Momchilov, A. Nassalevska, G. Pistoia, M. Pasquali, *J. Power Sources* 1995, 54, 501-507.
- [14] H. Liu, Y. Wang, L. Li, K. Wang, E. Hosono, H. Zhou, *J. Mater. Chem.* 2009, 19, 7885-7891.
- [15] Y. Xu, X. Han, L. Zheng, W. Yan, Y. Xie, *J. Mater. Chem.* 2011, 21, 14466-14472.
- [16] G. J. Wang, N. H. Zhao, L. C. Yang, Y. P. Wu, H. Q. Wu, R. Holze, *Electrochim. Acta* 2007, 52, 4911-4915.

- [17] aH. Heli, H. Yadegari, A. Jabbari, *Mater. Chem. Phys.* 2011, 126, 476-479; bA. Pan, J. G. Zhang, G. Cao, S. Liang, C. Wang, Z. Nie, B. W. Arey, W. Xu, D. Liu, J. Xiao, G. Li, J. Liu, *J. Mater. Chem.* 2011, 21, 10077-10084.
- [18] aK. Ohwada, T. Yamauchi, Y. Fujii, Y. Ueda, *Phys. Rev. B* 2012, 85, 134102; bR. Baddour-Hadjean, S. Bach, N. Emery, J. P. Pereira-Ramos, *J. Mater. Chem.* 2011, 21, 11296-11305.
- [19] A. Q. Pan, H. B. Wu, L. Zhang, X. W. Lou, *Energy Environ. Sci.* 2013, 6, 1476-1479.
- [20] J. Bao, M. Zhou, Y. Zeng, L. Bai, X. Zhang, K. Xu, Y. Xie, *J. Mater. Chem. A* 2013, 1, 5423-5429.
- [21] T. Khamaganova, V. Trunov, *Russ J. Inorg. Chem.* 1989, 34, 164-168.
- [22] P. Rozier, M. Morcrette, P. Martin, L. Laffont, J. M. Tarascon, *Chem. Mater.* 2005, 17, 984-991.
- [23] M. E. Spahr, P. Novák, W. Scheifele, O. Haas, R. Nesper, *J. Electrochem. Soc.* 1998, 145, 421-427.
- [24] G. Nagaraju, S. Sarkar, J. Dupont, S. Sampath, *Solid State Ionics* 2012, 227, 30-38.
- [25] E. Khoo, J. Wang, J. Ma, P. S. Lee, *J. Mater. Chem.* 2010, 20, 8368-8374.
- [26] J. Yu, J. C. Yu, *Mater. Chem. Phys.* 2007, 104, 362-366.
- [27] X. Xu, Y. Z. Luo, L. Q. Mai, Y. L. Zhao, Q. Y. An, L. Xu, F. Hu, L. Zhang, Q. J. Zhang, *NPG Asia Mater.* 2012, 4, e20.
- [28] H. Wang, S. Liu, Y. Ren, W. Wang, A. Tang, *Energy Environ. Sci.* 2012, 5, 6173-6179.
- [29] J. Kawakita, M. Majima, T. Miura, T. Kishi, *J. Power Sources* 1997, 66, 135-139.
- [30] aJ. Y. Luo, W. J. Cui, P. He, Y. Y. Xia, *Nat. Chem.* 2010, 2, 760-765; bY. Wang, Y. Xia, *J. Electrochem. Soc.* 2006, 153, A450-A454.
- [31] I. Stojkovic, N. Cvjeticanin, M. Mitric, S. Mentus, *Electrochim. Acta* 2011, 56, 6469-6473.
- [32] H. Wang, K. Huang, Y. Zeng, F. Zhao, L. Chen, *Electrochim. Solid-State Lett* 2007, 10, A199-A203.
- [33] H. Wang, Y. Zeng, K. Huang, S. Liu, L. Chen, *Electrochim. Acta* 2007, 52, 5102-5107.
- [34] L. Liu, M. Zhou, X. Wang, F. Tian, H. Guo, B. Shen, T. Hu, *J. Electrochem. Soc.* 2012, 159, A1230-A1235.
- [35] aL. L. Liu, X. J. Wang, Y. S. Zhu, C. L. Hu, Y. P. Wu, R. Holze, *J. Power Sources* 2013, 224, 290-294; bF. Nobili, F. Croce, B. Scrosati, R. Marassi, *Chem. Mater.* 2001, 13, 1642-1646.
- [36] aY. K. Sun, J. M. Han, S. T. Myung, S. W. Lee, K. Amine, *Electrochem. Commun.* 2006, 8, 821-826; bS. Yang, H. Song, X. Chen, A. V. Okotrub, L. G. Bulusheva, *Electrochim. Acta* 2007, 52, 5286-5293; cY. Sun, X. Hu, W. Luo, Y. Huang, *ACS Nano* 2011, 5, 7100-7107.
- [37] J. Fan, P. S. Fedkiw, *J. Power Sources* 1998, 72, 165-173.
- [38] H. Wang, K. Huang, C. Huang, S. Liu, Y. Ren, X. Huang, *J. Power Sources* 2011, 196, 5645-5650.
- [39] Q. Qu, L. Fu, X. Zhan, D. Samuelis, J. Maier, L. Li, S. Tian, Z. Li, Y. Wu, *Energy Environ. Sci.* 2011, 4, 3985-3990.
- [40] aY. Wang, X. Xu, C. Cao, C. Shi, W. Mo, H. Zhu, *J. Power Sources* 2013, 242, 230-235; bG. Yang, G. Wang, W. Hou, *J. Phys. Chem. B* 2005, 109, 11186-11196.
- [41] aH. Wang, H. He, N. Zhou, G. Jin, Y. Tang, *Trans. Nonferrous Met. Soc. China* 2014, 24(2), 415-422; bC. Q. Feng, S. Y. Chew, Z. P. Guo, J. Z. Wang, H. K. Liu, *J. Power Sources* 2007, 174, 1095-1099.
- [42] M. Shui, W. Zheng, J. Shu, Q. Wang, S. Gao, D. Xu, L. Chen, L. Feng, Y. Ren, *Mater. Res. Bul.* 2012, 47, 2455-2459.
- [43] J. Kawakita, T. Miura, T. Kishi, *Solid State Ionics* 1999, 118, 141-147.